



Research on the Influence of Yarn Reduction on the Bending Performance of Three-dimensional Woven Composites

Chao Li^{1,2} · Haili Zhou² · Yang Sun² · Fangfang Sun² · Zhiyan Liu² · Jian Huang² · Liqian Zhang² · Chengming Yue² · Qian Zhao² · Shoufu Yu² · Guangming Zhou¹

Received: 16 November 2023 / Accepted: 25 January 2024 / Published online: 29 February 2024
© The Author(s), under exclusive licence to Springer Nature B.V. 2024

Abstract

The primary objective of this study is to conduct a comprehensive experimental investigation into the impact of yarn reduction on the damage mechanisms and progression of 3D woven composites under bending loads, utilizing a combination of micro-XCT and digital image correlation (DIC) techniques. Typical bending behaviors of 3D woven composites have been discussed through load–displacement curves combining camera photography techniques. The influence of yarn reduction on strain distribution during bending deformation can be obtained by utilizing DIC techniques. Additionally, the final failure mode analysis of three-dimensional woven composite materials was conducted using micro-XCT techniques.

Keywords 3D woven composites · Yarn reduction · Three-point bending · Damage evolution

1 Introduction

Replacing metal materials with fiber reinforced polymer composites with low density, high strength, high modulus and excellent durability is an important means to achieve weight reduction of structural parts [1, 2]. Due to the complex integrated structure and flexible structural designability [3–5], 3D woven composites have outstanding advantages in near-net size molding and interlayer performance, and have been widely used in aerospace, automotive industry and other fields [6–8].

At present, the technique of yarn addition and reduction is the key technology for preparing complex structural parts with variable cross-section or thickness [9–11]. However, the introduction of yarn reduction will inevitably lead to local structural changes and then form defects in the prefabricated parts. Liu et al. [12–14] systematically studied the static

✉ Haili Zhou
zhouhaili420@163.com

✉ Qian Zhao
qzhao@fiberglasschina.com

¹ State Key Laboratory of Mechanics and Control for Aerospace Structures, Nanjing University of Aeronautics and Astronautics, Nanjing 210016, People's Republic of China

² Nanjing Fiberglass Research & Design Institute Co., Ltd, Nanjing 210012, People's Republic of China

tensile and tensile fatigue properties of 3D five-directional braided composite with yarn reduction structure, and the results showed that yarn reduction reduced the load bearing capacity of the materials. The stress concentration and failure of composites were easy to occur in the yarn reducing position, which seriously affected the service reliability of components. Dou et al. [15] compared the mechanical properties and progressive failure processes of 3D angle interlocking woven composites with half and full row yarn reduction under low velocity impact and found that yarn reduction reduced the performance of composites and caused the change of failure mode. Sun et al. [16] showed that the failure of specimen with yarn reduction was mainly related to yarn breakage and fiber damage. Overall, further study on the effect of yarn reduction on the mechanical properties of components and in-depth analysis of the damage evolution process will be helpful for rational development of high-performance special-shaped components.

Nowadays, a range of nondestructive testing techniques have been used to acquire and analysis the progressive damage behavior of composites, such as acoustic emission (AE), DIC and micro-XCT. Gao et al. [17] used AE to monitor the damage process of 3D orthogonal woven composites under quasi-static three-point bending loads. The result shown that the changes in AE signals could identify cumulative damage processes such as matrix cracking and fiber breakage, while obtained the critical loading levels of composites. Nevertheless, a single AE monitoring method fails to visualize the damage evolution effectively and intuitively [18, 19]. In contrast, the introduction of DIC and micro-XCT technology [20–22] can more intuitively monitor the strain field evolution of composites and characterize the mechanical behavior. Zhang et al. [23] and Jiao et al. [24] used DIC to obtain the surface strain fields of 3D layer-to-layer orthogonal interlocked textile composite and 3D interlayer interlocking woven composites respectively under quasi-static three-point bending and tensile loads. Zhou et al. [25] monitored the strain of 3D woven variable thickness composite under tensile load with DIC, and the results showed that the predicted uniform stiffness in the warpage direction decreased with the increase of thickness. Regrettably, DIC is limited to surface damage assessment and cannot capture any internal damage. Therefore, many researches on damage detection were combined with micro-XCT technology. It provides accurate 3D image information by reconstructing multiple tomography images, which helps to evaluate damage propagation and visualize the progressive damage process inside [26]. Ai et al. [27] used micro-XCT to collect 2D images containing comprehensive meso-geometric information in a 3D orthogonal woven composite, and performed statistical analysis on the volume fraction and positioning of void defects in the structure. Sun et al. [28] obtained the global and local strain distribution of the surface of 3D woven composites under short-beam shear load through multi-scale DIC. Combined with micro-XCT, they found that transverse cracks in the weft yarn and interface debonding were important causes of nonlinear segments in the load–displacement curve of specimens. The complementary information obtained by different observation methods is helpful to reveal the complex damage mechanism of 3D woven composites.

To sum up, it can be found from previous studies that the research on yarn reduction structure mainly focused on 3D braided composites, while the research on yarn reduction involving 3D woven composites was rarely reported. In addition, the initiation and evolution of damage caused by yarn reduction under bending load for composites designed with yarn reduction have not been clarified.

Given above issues, to evaluate the effect of yarn reduction on the mechanical properties of 3D woven composites, 3D woven composites with different yarn reduction positions and different yarn reduction layers were designed and prepared in this paper. The damage expansion and failure mechanism of 3D woven composites with different yarn

reduction types under bending load were systematically analyzed by using DIC techniques and micro-XCT in this study. This work has a certain reference value for product design of 3D woven composites with variable section.

2 Experimentation

2.1 Sample Preparation

In this study, samples were prepared using carbon fiber preform reinforced polymer composites. The preforms were fabricated using CCF800H-12 K carbon fiber (Weihai Expansion Fiber Co., Ltd) based on a three-dimensional woven process. This process involved two directions of yarn: warp yarn and weft yarn, with the warp yarn passing through different layers of weft yarn to form a layered network structure. As shown in Fig. 1 and Table 1, the designed prefabricated structures in this study consisted of surface structures and internal structures. The surface structures had a higher interlacing density compared to the internal structures. Each cell of the surface structure included four columns of yarn, while each cell of the internal structure included eight columns of yarn. The higher interlacing density of the surface structure enhanced the overall integrity of the prefabricated structure. Both warp and weft yarns were made of 3-strand yarn, i.e., 36 K. The warp yarn had a density of 6 yarns/cm, while the weft yarn had a density of 3 yarns/cm. The total number of warp layers was 9, and the total number of weft layers was 8. This study investigated the influence of yarn reduction positions and the number of yarn reductions on the three-point bending performance of the composite material. Five yarn reduction methods were employed for the prefabricated structures: (1) no yarn reduction (R-0-0), (2) one layer of yarn reduction at the second layer (R-1-2), (3) one layer of yarn reduction at the third layer (R-1-3), (4) one layer of yarn reduction at the fourth layer (R-1-4), and (5) two layers of yarn reduction at the third and fourth layers (R-2-3/4). During the yarn reduction process, both the warp yarn and weft yarn were simultaneously reduced, and the reduction area formed a rectangular shape with a width of six weft yarns.

Figure 2 shows the preparation process of the three-point bending test specimens. Firstly, the preform plate was prepared, then the RTM (Resin Transfer Molding) technique was used for composite material molding with PR520 resin, and finally, it was cut into dimensions of 230 mm × 32 mm × 9.3 mm. Each type of structure included at least 3 test specimens. Table 2

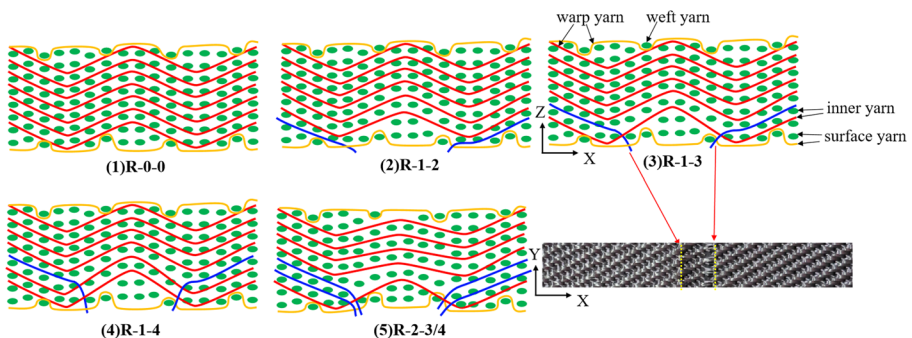


Fig. 1 The types of reduction yarn of 3D woven preform

Table 1 Preform structural parameters

Sample	Warp yarn		Weft yarn		Number of yarn reduction	Layer of yarn reduction
	Density (Threads/cm)	Number of filaments	Arrangement density (Threads/cm)	Number of filaments		
R-0-0	6	3 × 12 K	3	3 × 12 K	0	0
R-1-2	6	3 × 12 K	3	3 × 12 K	1	2
R-1-3	6	3 × 12 K	3	3 × 12 K	1	3
R-1-4	6	3 × 12 K	3	3 × 12 K	1	4
R-2-3/4	6	3 × 12 K	3	3 × 12 K	2	3/4

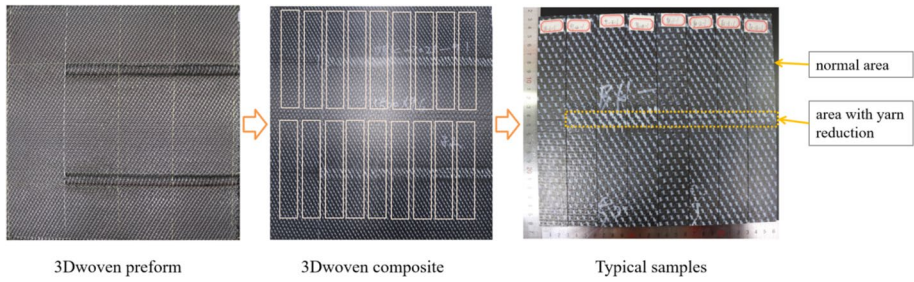


Fig. 2 The types of reduction yarn of 3D woven preform

shows the parameters of various types of test specimens. The fiber volume fraction of the three-dimensional woven composite material is approximately 62%. However, in the yarn reduction region, the fiber volume fraction is lower due to the removal of yarns. The fiber volume fraction is approximately 55% when one layer of yarn was removed, and approximately 48% when two layers of yarn were removed.

2.2 Bending Test

The three-point bending test was conducted according to ASTM D7264 standard. The span-to-thickness ratio of the specimen was approximately 16:1, with a span of 154 mm. The bending loading rate was set at 4 mm/min. The warp direction of the composite material was in the length direction. As shown in Fig. 3, for specimens with yarn reduction, ensure that the line of yarn reduction was positioned at the bottom surface of the specimen and directly below the loading head. The testing equipment used was the ITW Group Instron Model 5982/100kN electronic universal testing machine. The bending strength and bending modulus were calculated using the following formulas:

$$\sigma_f = 3PL/2bh^2 \tag{1}$$

$$E_f = L^3m/4bh^3 \tag{2}$$

Table 2 Composite parameters

Sample	Thickness		Width		Vf (normal area)		Vf (area with yarn reduction)	
	Mean (mm)	CV (%)	Mean (mm)	CV (%)	Mean (%)	CV (%)	Mean (%)	CV (%)
R-0-0	9.29	0.64	32.08	0.40	62.11	0.70	/	/
R-1-2	9.21	0.46	32.14	0.45	62.37	0.46	54.93	0.39
R-1-3	9.24	0.54	32.23	1.02	62.65	0.55	55.45	0.54
R-1-4	9.37	0.13	32.26	0.46	63.17	0.12	55.91	0.13
R-2-3/4	9.38	0.77	32.15	0.07	62.08	0.77	47.80	0.77

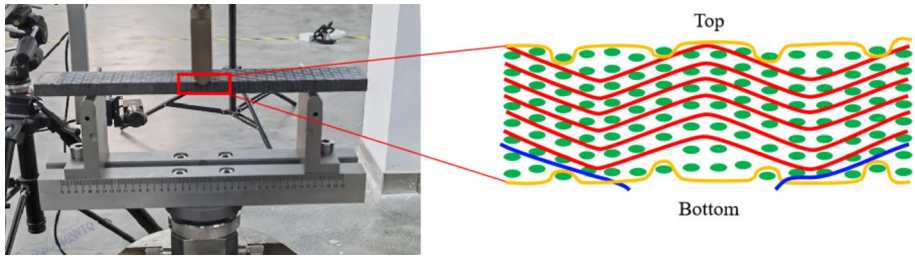


Fig. 3 3-point bending test of 3D woven composite

where P is the maximum load, L is the support span, b is the specimen width, h is the specimen thickness, and m is the slope of the load–displacement curve.

2.3 Digital Image Correlation

The DIC full-field strain measurement system (VIC-3D) from Correlated Solutions Europe in Germany was used to obtain surface strain fields in a tensile experiment. The DIC system utilized CCD cameras with a sampling rate of 3 frames per second during the test. The strain measurement accuracy of the system was $3D \leq 50\mu\epsilon$ and $2D \leq 10\mu\epsilon$. The strain measurement range was $0.005\% \sim \geq 2000\%$, and the noise of the strain measurement system was $3D \leq 20\mu\epsilon$. Prior to the test, the top surface of the specimen was coated with a speckle pattern. The results were post-processed using the ARAMIS professional software provided by the system manufacturer to obtain the evolution of surface strain fields throughout the entire tensile testing process.

2.4 Micro-XCT Test

The three-dimensional XCT measurement is performed using the D2 computer tomography scanner from DIONDO, Germany, equipped with a 240 kV nano-focus X-ray tube. The sample with phase damage has been exposed to radiation and two-dimensional slice images are obtained through a 360° rotation for three-dimensional reconstruction. The focal spot size of the nano-focus X-ray tube is $0.5 \mu\text{m}$. After the test is completed, the damaged area in the scanned sample is analyzed. The three-dimensional reconstruction of cracks along the latitude, longitude, and thickness directions is analyzed to determine the damage status.

3 Results and Discussions

3.1 The Influence of Yarn Reduction on Material Bending Performance

The load–displacement curves for three-point bending of 3D woven composite specimens with different yarn reduction patterns are shown in Fig. 4. The curves for all five structures exhibit similar trends, consisting of three stages: linear stage, nonlinear increasing stage, and nonlinear decreasing stage. The displacements corresponding to each stage are similar, but there are differences in the load values. The no yarn reduction

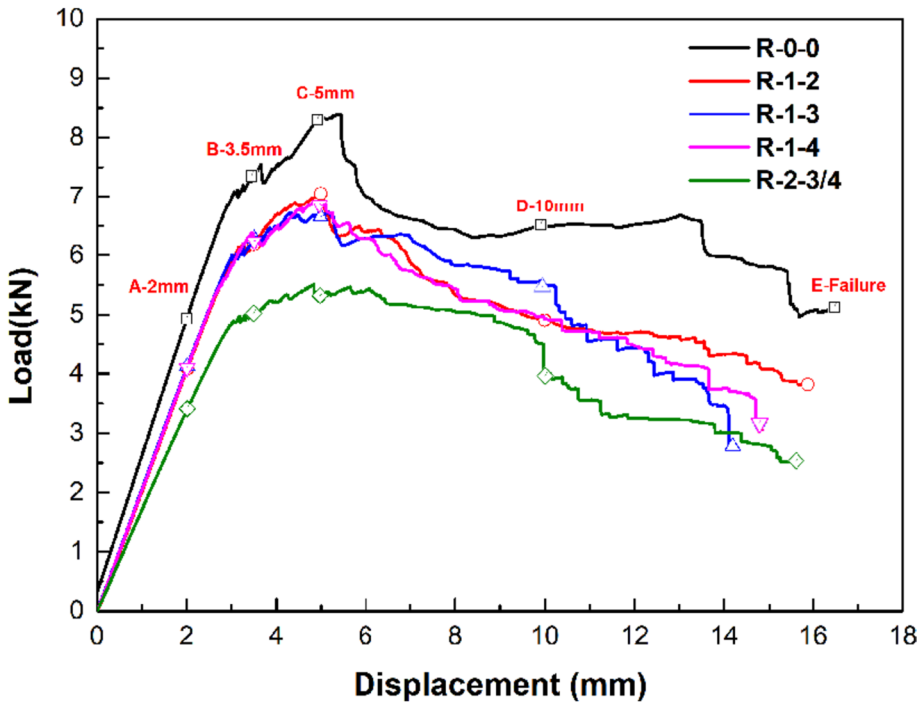


Fig. 4 The types of reduction yarn of 3D woven preform

(R-0-0) structure has a higher load level than the structures with one yarn reduction (R-1-2~4) or two yarn reductions (R-2-3/4). Among the structures with one yarn reduction, the load levels are similar regardless of the position of the reduction (R-1-2~4).

As shown in Fig. 5, the maximum loads for the five structures are compared. The number of yarn reductions has a significant impact on the maximum load, while the position of the yarn reduction has little effect when the same number of yarns are reduced. The maximum load for the no yarn reduction (R-0-0) structure is 7.6 kN. For the structures with one yarn reduction (R-1-2~4), the maximum load slightly increases as the reduction position moves towards the thickness center, ranging from 6.88 to 6.96 kN, which is 8.4% to 9.5% lower than the no yarn reduction structure. The structure with two yarn reductions has a maximum load of 5.73 kN, which is 24.6% lower than the no-yarn reduction structure.

Figure 6 compares the flexural strength and flexural modulus of the different structures. The influence of yarn reduction on flexural strength and flexural modulus is similar to its influence on the maximum load. As the number of yarn reductions increases, the flexural strength and flexural modulus decrease. The reduction of one yarn has a small effect on the flexural strength and modulus when its position varies in the thickness. The values slightly increase as the reduction position moves towards the center. The flexural strength and modulus of the no yarn reduction specimen are 623.04 MPa and 81.42 GPa, respectively. For the specimens with one yarn reduction, the flexural strength ranges from 568.17 to 586.92 MPa, and the flexural modulus ranges from 73.38 to 74.41 GPa, which are 8.8% to 5.8% and 9.9% to 8.6% lower than the no yarn

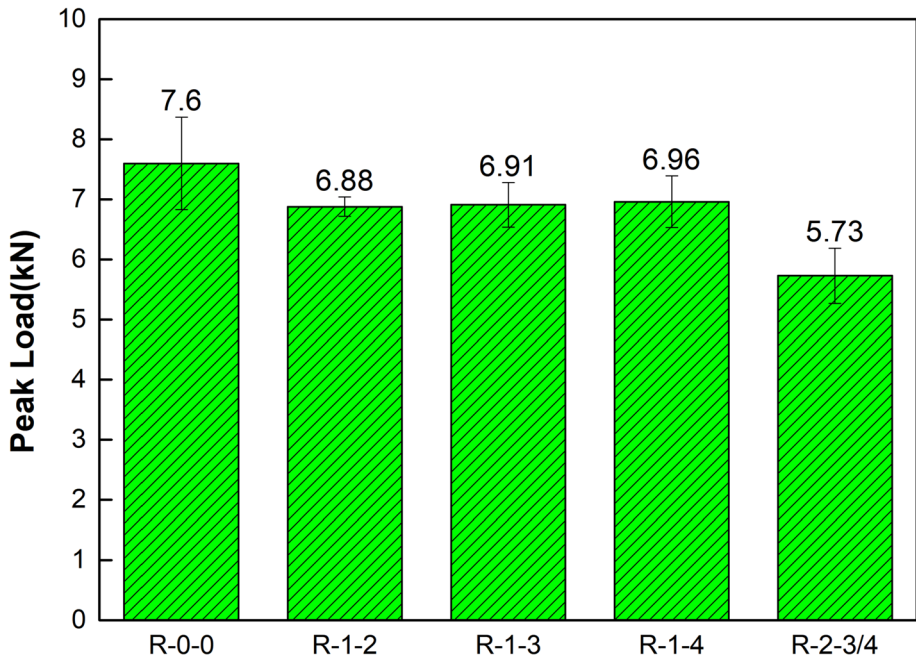


Fig. 5 Peak load of 3D woven composite with different types of yarn reduction

reduction specimen, respectively. The flexural strength and modulus of the specimen with two yarn reductions are 468.29 MPa and 62.84 GPa, respectively, which are 24.8% and 22.8% lower than the no yarn reduction specimen.

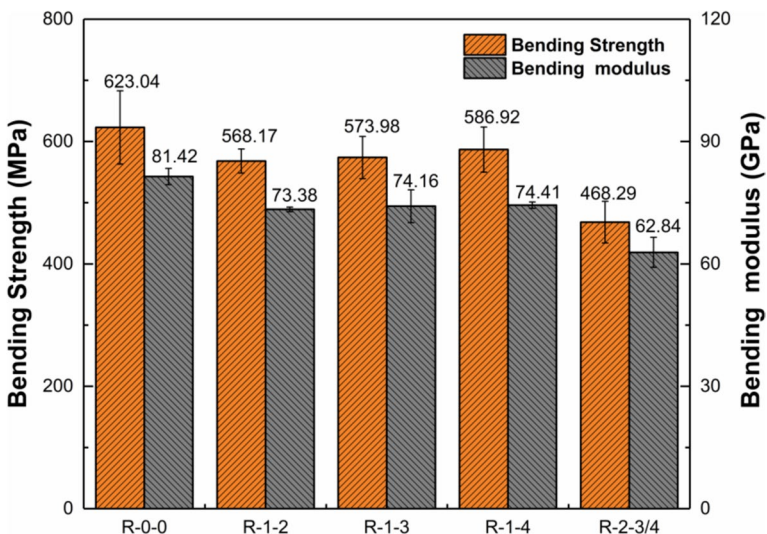


Fig. 6 Bending strength and modulus of 3D woven composite with different types of yarn reduction

In conclusion, the number of yarn reductions has a significant impact on the flexural performance of 3D woven composite materials, while the position of the yarn reduction has a minimal effect.

3.2 The Influence of Yarn Reduction on the Bending Failure Process

Figures 7, 8 and 9 demonstrate the deformation and progressive damage evolution of different yarn-reduced three-dimensional woven composite specimens under three-point bending loading. During the loading process, the deformation and failure processes of one side of the specimens were recorded using a camera, while the strain variations were measured using Digital Image Correlation (DIC) on the other side. Three markers on the side of the specimen represent the positions of the yarn reduction on both sides and the center loading point.

Five deformation positions (A–E) were selected for comparison among different structural specimens during the loading process (2 mm, 3.5 mm, 5 mm, 10 mm, and final failure). Point A is in the linear stage of the load-displacement curve, while point B represents the onset of yielding, point C is near the maximum load, and point D is in the load-decreasing stage.

From Fig. 8, it can be observed that at position A, there is minimal damage on the side of the specimen. At point B, cracks and resin cracking occur on both sides of the compressed surface, and yielding is observed, indicating the transition to the nonlinear stage. At point C, cracks on the compressed surface extend from the side surface downward toward the compressed center, and fiber fracture occurs. At the same time, resin cracks appear on the tension surface below. More cracks are observed at point D, with further extension of the original cracks and extensive yarn breakage. At point E, complete failure occurs, with cracks on the upper surface extending to the center of the loading head and the central yarn on the tension surface below being pulled apart.

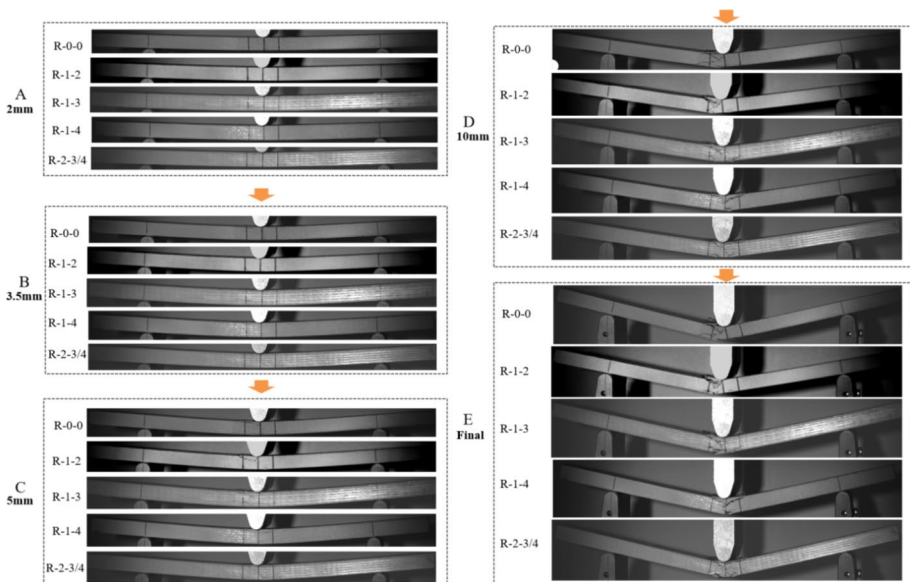


Fig. 7 Three-point bending deformation process

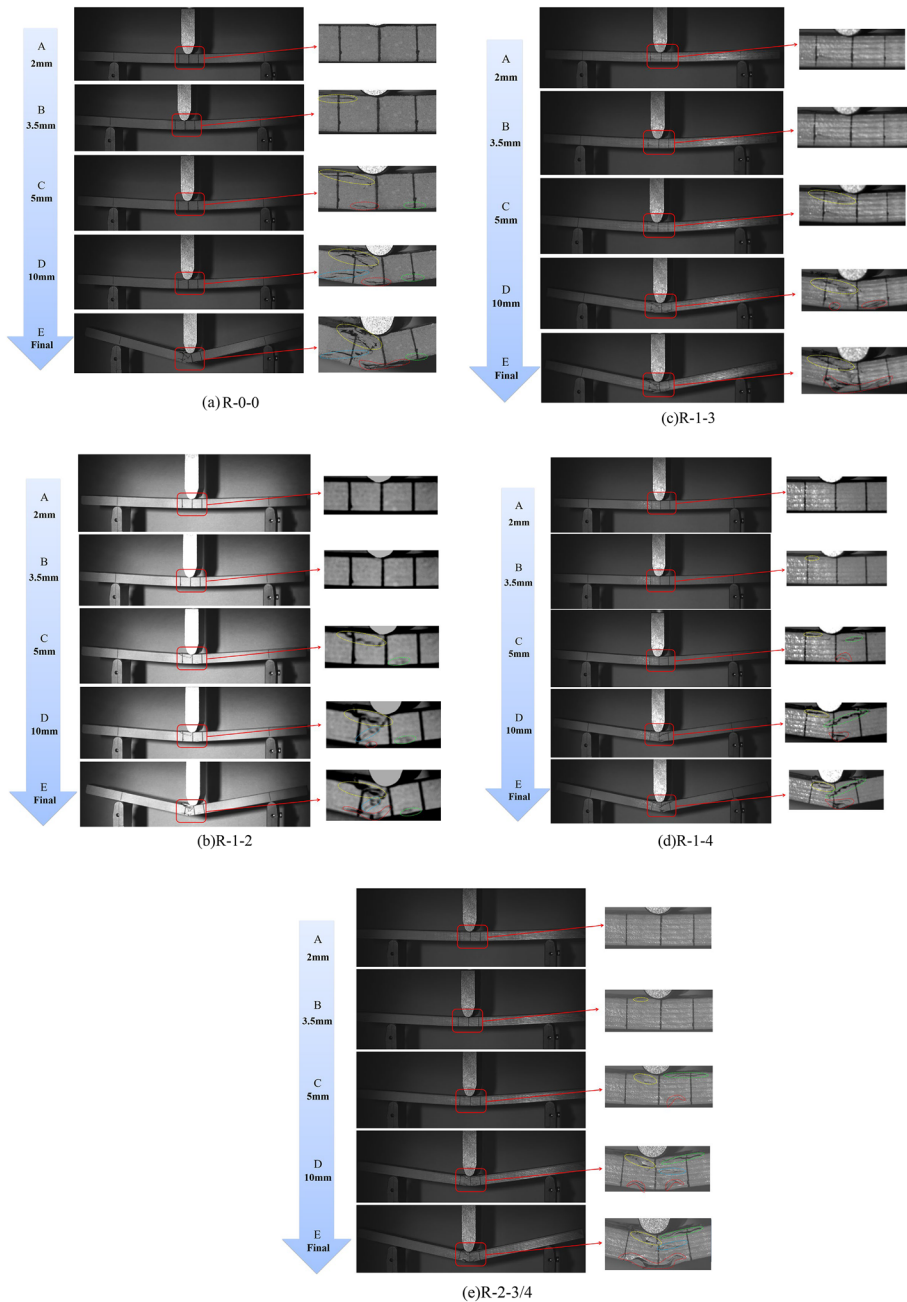


Fig. 8 Evolution of damage in three-point bending of sample

Figure 9 compares the strain distributions at points B and C during the three-point bending test for different yarn reduction methods. The specimens exhibit similar patterns below the loading head, with compression on the upper surface and tension on the lower surface.

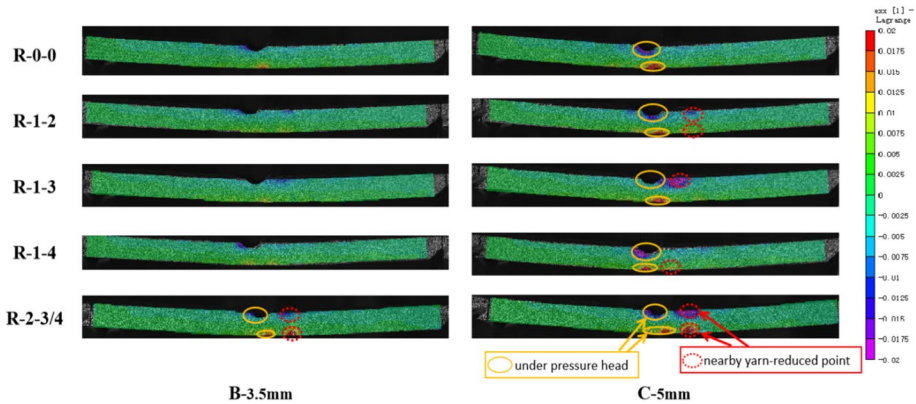


Fig. 9 Digital Image Correlation (DIC) strain field

The stress concentration areas are located below the pressure head and on both sides of the pressure head in all specimens. Among them, in the specimens containing reduced yarns, the stress concentration is more pronounced on both sides of the pressure head. The reduction of one yarn layer at the second layer (R-1-2) and the reduction of two yarn layers at the third and fourth layers (R-2-3/4) show significant strain concentration at the reduction points, especially at point B, where noticeable strain concentration is observed at the reduction points, and the concentrated area expands at point C. On the other hand, reducing one yarn layer at the third and fourth layers shows minor influence at the reduction points, indicating that offsetting the reduction points towards the center in the thickness direction can alleviate strain concentration on the surface.

3.3 Analysis of Bending Failure Modes

Figure 10 shows the CT images of local damage after testing different types of specimens. Three cross-sections were selected for analysis: A-A along the warp direction, which is the midpoint of the specimen width; B-B in the weft direction, on the side of the pressure head; C-C in the weft direction, directly beneath the pressure head.

From the A-A cross-section, it can be observed that the warp threads on the upper surface experienced more severe damage due to compression, while the lower surface showed more damage due to tension. The crack propagation direction was diagonally downward from the pressure head, extending from the upper surface through the thickness to the middle layer. Cracks on the lower surface were mainly concentrated directly beneath the pressure head, and fiber fracture primarily occurred in the surface layer.

On the B-B cross-section, the upper surface exhibited obvious interface delamination between the yarns and the resin forming a big crack. The delamination around the yarn and along the warp path showed a wavy pattern, indicating that the fiber paths in the three-dimensional woven structure hinder the resin cracking to some extent.

On the C-C cross-section, resin fragmentation was observed and there was a higher number of interface delaminations. The delamination profiles between the warp and weft yarns were distinct, and the R-2-3/4 specimen with two fewer yarn layers showed more severe internal damage.

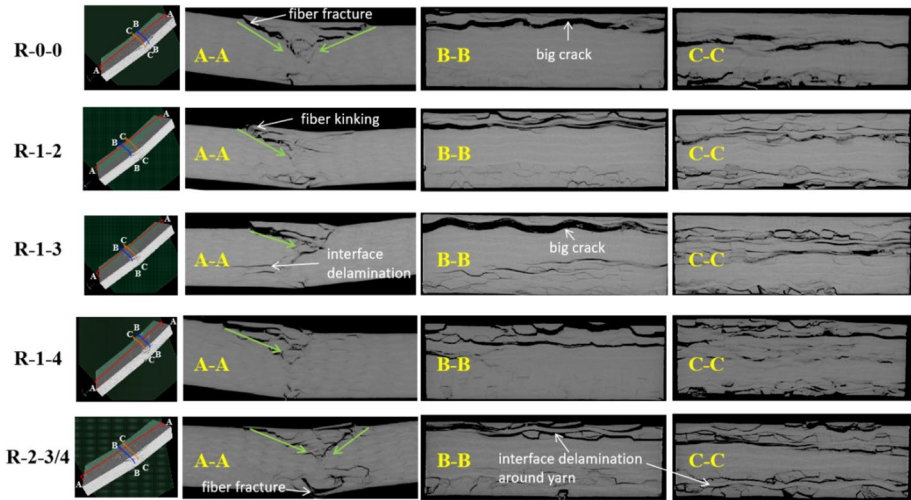


Fig. 10 Damage CT image of composite

These observations indicate that yarn fracture, resin cracking, and interface delamination are common types of damage. These damages lead to a reduction in the material's strength and stiffness, thereby affecting its mechanical performance. These analytical results are of significant importance for further research and improvement of the performance of three-dimensional woven composites.

4 Conclusions

In conclusion, this study investigated the influence of yarn reduction on the bending performance and failure modes of three-dimensional woven composite materials. The results showed that the quantity of yarn reduction significantly affected the bending strength and modulus, with an increase in the quantity of yarn reduction leading to a decrease in both bending strength and modulus. The position of yarn reduction had a minor impact on the bending performance, with a complete increase in strength and modulus observed when reducing one layer of yarn from the surface to the inner layers (from the 2nd to the 4th layer). In the specimens without yarn reduction, there was no strain concentration at the yarn reduction points on both sides, while strain concentration occurred at the yarn reduction points in other samples. Significant strain concentration was observed at the yarn reduction points when reducing one layer of yarn at the 2nd layer (R-1-2) and when reducing two layers of yarn at the 2nd and 3rd/4th layers (R-2-3/4). However, reducing one layer of yarn at the 3rd and 4th layers had a minor impact at the yarn reduction points, indicating that offsetting the yarn reduction points towards the center in the thickness direction could alleviate surface strain concentration. The bending failure process involved crack formation and propagation, interfacial delamination, and yarn fracture. Yarn fracture was more severe on the compression side, exhibiting diagonal shear failure, while yarn fracture occurred on the tension side mainly at the surface, primarily resulting from pulling from the compressed center position. These research findings provide valuable insights for future research and development of three-dimensional woven composite materials.

Author Contributions Chao Li, Haili Zhou and Chengming Yue wrote the manuscript text. Zhiyan Liu prepared the 3D woven preforms and Fig. 1. Yang Sun, Jian Huang completed the 3-point test and prepared Fig. 2. Fangfang Sun and Qian Zhao prepared Figs. 7, 8, and 9. Shoufu Yu prepared Tables 1 and 2. Guangming Zhou responsible for writing and editing relevant text for the paper. All authors reviewed the manuscript.

Funding The authors acknowledge the financial support from the Natural Science Foundation of Jiangsu Province (Grants No BK20220167, BK20220165, BK20222017) and the Young Elite Scientists Sponsorship Program by CAST (2022QNRC001).

Data Availability No datasets were generated or analysed during the current study.

Declarations

Competing Interests The authors declare no competing interests.

References

1. Rajak, D.K., Pagar, D.D., Menezes, P.L., Linul, E.: Fiber-reinforced polymer composites: Manufacturing, properties, and applications. *Polymers* **11**(10), 1667 (2019)
2. Chen, Y.L., Zhang, J.M., Li, Z.F., Zhang, H.L., Chen, J.P., Yang, W.D., et al.: Intelligent methods for optimization design of lightweight fiber-reinforced composite structures: A review and the-state-of-the-art. *Front. Mater. Sec. Mater. Sec. Polym. Compos. Mater.* **10**, 1–5 (2023)
3. Huang, T., Wang, Y.L., Wang, G.: Review of the Mechanical properties of a 3D Woven Composite and its applications. *Polym-Plast. Technol. Eng.* **57**, 740–756 (2018)
4. Korkmaz, M., Okur, A.: The review about the numerical modelling and analysis of 3D woven fabrics. *J. Text. Inst.* **114**, 496–522 (2023)
5. Umair, M., Hamdani, S.T.A., Hussain, M., Nawab, Y.: Mechanical performance of 3D woven jute/green epoxy composites with novel weaving patterns. *J. Ind. Text.* **51**, 5794S–5821S (2022)
6. Liu, L.L., Shao, H.Y., Zhu, X.Y., Zhao, Z.H., Zhang, G., Luo, G., et al.: Bird impact response and damage mechanism of 3D orthogonal woven composite aeroengine blades. *Compos. Struct.* **304**, 116311 (2023)
7. Foti, F., Pannier, Y., Balaciart, S.O., Grandidier, J.-C., Gigliotti, M., Guigon, C.: In-situ multi-axial testing of three-dimensional (3D) woven organic matrix composites for aeroengine applications. *Compos. Struct.* **273**, 114259 (2021)
8. Behera, B.K., Kamble, Z.: Advanced 3D woven profile structures and their composites for automotive applications. *Polym. Compos.* **43**, 5946–5953 (2022)
9. Liu, Z.L., Liu, L.F., Yu, J.Y.: Net shape preparation and bending properties of tapered three-dimensional braided composites. *Text. Res. J.* **82**, 1870–1879 (2012)
10. Liu, Z., Liu, L., Yu, J.: Unit yarn-reduction technique and flexural properties of tapered composites based on four-step row and column braiding. *Compos. Part A Appl. Sci. Manufac.* **42**, 1883–1891 (2011)
11. Ma, W.S., Zhu, J.X., Jiang, Y.: Studies of fiber volume fraction and geometry of variable cross-section tubular 3D five-direction braided fabric. *J. Compos. Mater.* **46**, 1697–1704 (2012)
12. Liu, X., Zhang, D., Mao, C., Wang, X., Qian, K.: Full-field progressive fatigue damage of 3D5D braided composites with yarn-reduction: Visualization, classification, and quantification. *Compos. Sci. Technol.* **218**, 109214 (2022)
13. Liu, X., Zhang, D., Qiu, H., Sun, J., Mao, C., Qian, K.: On-axis fatigue behaviors and failure characterization of 3D5D braided composites with yarn-reduction using X-ray computed tomography. *Compos. Sci. Technol.* **203**, 108585 (2021)
14. Liu, X., Ge, J., Wang, X., Qian, K., Liang, J., Zhang, D.: Multiscale image-based modeling of progressive damage in 3D5D braided composites with yarn-reduction. *Int. J. Solids Struct.* **270**, 112236 (2023)
15. Dou, H., Yang, Y., Sun, M., Zhang, D.: Effect of yarn reduction types on the mechanical response and damage mechanism of 3D woven composites subjected to low-velocity impact. *Appl. Compos. Mater.* **30**, 1415–1433 (2023)
16. Sun, M., Liu, X., Zhang, D., Sun, J., Qian, K.: Effects of structural defects on low-velocity impact damage mechanisms of three-dimensional braided composites based on X-ray micro-computed tomography. *Polym. Test.* **104**, 107403 (2021)

17. Gao, X., Tao, N., Yang, X., Wang, C., Xu, F.: Quasi-static three-point bending and fatigue behavior of 3-D orthogonal woven composites. *Compos. Part B: Eng.* **159**, 173–183 (2019)
18. Zhou, W., Pan, Z., Wang, J., Qiao, S., Ma, L., Liu, J., et al.: Review on acoustic emission source location, damage recognition and lifetime prediction of fiber-reinforced composites. *J. Mater. Sci.* **58**, 583–607 (2023)
19. Maillat, E., Baker, C., Morscher, G.N., Pujar, V.V., Lemanski, J.R.: Feasibility and limitations of damage identification in composite materials using acoustic emission. *Compos. Part A: Appl. Sci. Manufac.* **75**, 77–83 (2015)
20. Liu, H., Liu, J., Ding, Y., Zhou, J., Kong, X., Harper, L.T., et al.: Modelling damage in fibre-reinforced thermoplastic composite laminates subjected to three-point bend loading. *Compos. Struct.* **236**, 111889 (2020)
21. Liang, Q., Liu, J., Wang, X., Liu, X., Zhang, D., Qian, K.: Flexural progressive failure mechanism of hybrid 3D woven composites: Combination of X-ray tomography, acoustic emission and digital image correlation. *Compos. Struct.* **280**, 114894 (2022)
22. Han, K.N., Zhou, W., Qin, R., Yang, S., Ma, L.H.: Progressive damage analysis of carbon fabric-reinforced polymer composites under three-point bending. *Fibers Polym.* **22**, 469–479 (2021)
23. Zhang, D., Waas, A.M., Pankow, M., Yen, C.F., Ghiorse, S.: Flexural behavior of a layer-to-layer orthogonal interlocked three-dimensional textile composite. *J. Eng. Mater. Technology-Transactions Asme.* **134**(3), 031009 (2012)
24. Jiao, W., Chen, L., Xie, J., Yang, Z., Fang, J., Chen, L.: Effect of weaving structures on the geometry variations and mechanical properties of 3D LTL woven composites. *Compos. Struct.* **252**, 112756 (2020)
25. Zhou, Y., Cui, H., Wen, W.: Mechanical behavior of 3D woven variable thickness composite plate under tensile loading. *Fibers Polym.* **23**, 819–826 (2022)
26. Zhang, P.F., Zhou, W., Yin, H.F., Shang, Y.J.: Progressive damage analysis of three-dimensional braided composites under flexural load by micro-CT and acoustic emission. *Compos. Struct.* **226**, 111196 (2019)
27. Ai, S.G., Zhu, X.L., Mao, Y.Q., Pei, Y.M., Fang, D.N.: Finite element modeling of 3D orthogonal woven C/C composite based on micro-computed tomography experiment. *Appl. Compos. Mater.* **21**, 603–614 (2014)
28. Sun, R., Zheng, T., Yao, Y., Li, D., Si, H., Guo, L.: Experimental investigation on shear damage evolution of 3D woven composites using in situ computed tomography and multi-scale digital image correlation. *Compos. Struct.* **319**, 117159 (2023)

Publisher's Note Springer Nature remains neutral with regard to jurisdictional claims in published maps and institutional affiliations.

Springer Nature or its licensor (e.g. a society or other partner) holds exclusive rights to this article under a publishing agreement with the author(s) or other rightsholder(s); author self-archiving of the accepted manuscript version of this article is solely governed by the terms of such publishing agreement and applicable law.